

Supporting Information

for

Electron Delocalization from the Fullerene Attachment to the Diiron Core within the Active Site Mimics of [FeFe]-Hydrogenase

Yu-Chiao Liu,[†] Tao-Hung Yen,^{†,‡} Yu-Jan Tseng,[§] Ching-Han Hu,[§] Gene-Hsiang Lee[◇] and Ming-Hsi Chiang^{*,†,‡}

* To whom correspondence should be addressed. E-mail: mhchiang@chem.sinica.edu.tw.

[†] Institute of Chemistry, Academia Sinica, Nankang, Taipei 115, Taiwan

[‡] Molecular Science and Technology Program, TIGP, Institute of Chemistry, Academia Sinica, Nankang, Taipei 115, Taiwan

[§] Department of Chemistry, National Changhua University of Education, Changhua 500, Taiwan

[◇] Instrumentation Center, National Taiwan University, Taipei 106, Taiwan

Contents

I. Experimental Section

II. Table

Table S1. X-ray crystallographic data.

Table S2. List of the electrochemical data.

III. Figures

Figure S1. Molecular structure of $[(\mu\text{-bdt})\text{Fe}_2(\text{CO})_5(\text{PPh}_3)]$, **2**.

Figure S2. Cyclic voltammograms of **1** in the anodic region.

Figure S3. Cyclic voltammogram of $[(\mu\text{-bdt})\text{Fe}_2(\text{CO})_6]$.

Figure S4. IR spectra of **1** and $[\mathbf{1}]^{\text{Tm}}$ in THF solution at $-50\text{ }^\circ\text{C}$.

Figure S5. 77 K EPR spectra of (a) $[\mathbf{1}]^{\text{Tm}}$ and (b) $[\mathbf{3}]^-$ in THF. The in-situ vis-NIR spectra of (c) $[\mathbf{1}]^{\text{Tm}}$ and (d) $[\mathbf{3}]^-$ in THF at $-70\text{ }^\circ\text{C}$.

Figure S6. The vis-NIR spectral change of $[\mathbf{1}]^{\text{Tm}}$ upon addition of (a) HCl and (b) HOAc in the THF solution at $-50\text{ }^\circ\text{C}$.

Figure S7. The calculation results of **1**, $[\mathbf{1}]^{\text{Tm}}$ and $[\mathbf{1}]^{2\text{Tm}}$.

Figure S8. Cyclic voltammograms of **2**.

Figure S9. NMR spectra of **1**.

IV. References

I. Experimental Section

General Methods. All reactions were carried out by using standard Schlenk and vacuum-line techniques under an atmosphere of purified nitrogen. All commercial available chemicals from Aldrich were of ACS grade and used without further purification. Solvents were of HPLC grade and purified as follows: hexane, diethyl ether and THF (tetrahydrofuran) were distilled from sodium/benzophenone under N₂. Dichloromethane was distilled from CaH₂ under N₂. Acetonitrile was distilled first over CaH₂ and then from P₂O₅ under N₂. TFA (trifluoroacetic acid) and *o*-DCB (*o*-dichlorobenzene) were distilled from P₂O₅ under N₂. Deuterated solvents obtained from Merck were distilled over 4 Å molecular sieves under N₂ prior to use. [(μ-bdt)Fe₂(CO)₆],¹ C₆₀(H)PPh₂² and H₃BC₆₀(H)PPh₂² were prepared according to related literature procedures.

Infrared spectra were recorded on a Perkin Elmer Spectrum One using a 0.05-mm CaF₂ cell. ¹H, ¹³C{¹H} and ³¹P{¹H} NMR spectra were recorded on a Bruker AV-500 or DRX-500 spectrometer operating at 500, 125.7 and 202.49 MHz, respectively. In-situ UV-vis spectra were recorded on a Varian Cary 5000 spectrophotometer equipped a Hellma All-Quartz Immersion Probes (661.302) at low temperature. Mass spectral analyses were done on a Waters LCT Premier XE at Mass Spectrometry Center in Institute of Chemistry, Academia Sinica. Elemental analyses were performed on an Elementar vario EL III elemental analyzer. Analysis of H₂ gas from bulk electrolysis was performed on an Agilent 6890 gas chromatograph with a TCD detector and a Supelco Carboxen 1000 column. Argon was used as the carrier gas. X-band EPR measurements were performed at 77 K on a Bruker EMX spectrometer equipped with a Bruker TE102 cavity.

Molecular Structure Determinations. The X-ray single crystal crystallographic data collections for **1** (CCDC 853545) and **2** (CCDC 853546) were carried out at 150 K on a Bruker SMART APEX CCD four-circle diffractometer with graphite-monochromated Mo K α radiation ($\lambda = 0.71073 \text{ \AA}$) outfitted with a low-temperature, nitrogen-stream aperture. The structures were solved using direct methods, in conjunction with standard difference Fourier techniques and refined by full-matrix least-squares procedures. A summary of the crystallographic data for complexes **1** and **2** is shown in Table S1. Selected metric data of each structure are listed in figure captions. An empirical absorption correction (multi-scan) was applied to the diffraction data for all structures. All non-hydrogen atoms were refined anisotropically and all hydrogen atoms were placed in geometrically calculated positions by the riding model. All software used for diffraction data processing and crystal structure solution and refinement are contained in the SHELXTL97 program suites.³

Electrochemistry. Electrochemical measurements were recorded on a CH Instruments 630C electrochemical potentiostat using a gastight three-electrode cell under N₂ at room temperature. A glassy carbon electrode (3 mm in diameter) and a platinum wire were used as working and auxiliary electrode, respectively. Reference electrode was a non-aqueous Ag/Ag⁺ electrode (0.01 M AgNO₃/0.1 M *n*-Bu₄NPF₆). All potentials are measured in 0.1 M *n*-Bu₄NPF₆ solution in CH₂Cl₂/*o*-DCB (v/v 1/1) and reported against ferrocene/ferrocenium (Fc/Fc⁺). Insolubility of **1** in most of common organic solvents including CH₃CN and DMF (dimethylformamide) prohibits the electrochemical measurements in such solution. The complex **1** is slightly soluble in CH₂Cl₂. The theoretical ΔE value (the difference of E_{pc} and E_{pa}) for the reversible 1 electron redox

reaction is 59 mV. Low conductivity in the CH₂Cl₂/*o*-DCB (v/v 1/1) solution results in a large peak separation (120 mV) for the Fc/Fc⁺ pair.

Spectroelectrochemistry was performed by a Mettler Toledo ReactIR iC10 in situ FTIR system equipped with a MCT detector and a 0.625-in SiComp probe. Graphite rods (6.15 mm in diameter) were used as working and auxiliary electrodes. Reference electrode was a non-aqueous Ag/Ag⁺ electrode (0.01 M AgNO₃/0.1 M *n*-Bu₄NPF₆). The auxiliary and reference electrodes were placed in separated compartments with a fine porosity glass frit. The solution was stirred under N₂ throughout bulk electrolysis.

Computational Details. The geometries of the neutral, anion, and doubly anion (singlet and triplet states) complexes were optimized, and the vibrational frequencies of these species were computed. We used the three-parameter hybrid of exact exchange and Becke's exchange energy functional,⁴ plus Lee, Yang, and Parr's gradient-corrected correlation energy functional (B3LYP).⁵ The 6-31G(d) basis set was applied to all atoms. The Gaussian03 suite of programs was used in our study.⁶

For the doubly charged anion, we found that the triplet state is lower in energy than the singlet by 9.2 kcal/mol (ΔH at 298 K). The spin density, the frontier molecular orbitals and their corresponding energies of the neutral, single-charged and double-charged species are shown in the main text and support information section.

Synthesis of [(μ -bdt)Fe₂(CO)₅(C₆₀(H)PPh₂)], **1.** To a CH₂Cl₂ solution (5 mL) of [(μ -bdt)Fe₂(CO)₆] (100 mg, 0.24 mmol) was added an CH₃CN solution (5 mL) of Me₃NO (18 mg, 0.24 mmol). An instant color change was observed from red to dark red-brown. The solution was stirred for half an hour and then was concentrated to about one third of the volume. It was transferred to a Schlenk flask containing C₆₀(H)PPh₂ (218 mg, 0.24 mmol)

via cannula. The solution was stirred for one hour after addition of 30 mL of CS₂. The solution was evaporated to dryness and was subjected to column chromatography on silica gel. CS₂ was used as the eluent. The first band in purple which was C₆₀ was discarded. From the second band, a red solid was obtained. It was washed with several portions of CS₂/diethyl ether prior to being dried under vacuum. The yield was 105 mg (34 %). Crystals of [(μ-bdt)Fe₂(CO)₅(C₆₀(H)PPh₂)]·CS₂ suitable for X-ray crystallographic analysis were grown from a CS₂/hexane solution at -20 °C. IR (THF, cm⁻¹): ν_{CO} 2053 (vs), 1995 (vs), 1985 (s, sh), 1941 (w). ¹H NMR (500 MHz, CDCl₃, 298 K): 6.48 (m, 2H, S₂C₆H₄), 6.63 (s, 2H, S₂C₆H₄), 6.97 (d, ³J_{PH} = 22 Hz, 1H, C₆₀(H)PPh₂), 7.55 (m, 6H, *m*-/*p*-H, C₆₀(H)P(C₆H₅)₂), 8.29 (t, 4H, *o*-H, C₆₀(H)P(C₆H₅)₂) ppm. ¹³C{¹H} NMR (125.7 MHz, CDCl₃/CS₂ (v/v = 1/1), 298 K): 59.34 (d, 1C, J_{PC} = 8.2 Hz, C₆₀), 71.31 (d, 1C, J_{PC} = 12.6 Hz, C₆₀), 126.10 (s, 2C, S₂C₆H₄), 127.99 (s, 2C, S₂C₆H₄), 128.72 (d, 4C, J_{PC} = 8.7 Hz, C₆₀(H)P(C₆H₅)₂), 130.98 (d, 2C, C₆₀(H)P(C₆H₅)₂), 134.47 (d, 4C, J_{PC} = 9.8 Hz, C₆₀(H)P(C₆H₅)₂), 135.72 (d, J_{PC} = 31.1 Hz, 2C), 136.15 (2C), 137.46 (d, J_{PC} = 4.5 Hz, 2C), 139.03 (2C), 140.63 (2C), 141.29 (2C), 141.80 (2C), 141.98 (2C), 142.02 (2C), 142.33 (2C), 142.91 (2C), 142.99 (2C), 143.51 (2C), 144.73 (2C), 144.98 (2C), 145.59 (2C), 145.67 (2C), 145.80 (2C), 145.90 (2C), 145.99 (2C), 146.47 (2C), 146.49 (2C), 146.68 (2C), 146.72 (2C), 146.79 (2C), 147.55 (d, J_{PC} = 8.9 Hz, 2C), 147.88 (2C), 149.47 (2C), 151.10 (2C), 153.30 (d, J_{PC} = 3.9 Hz, 2C), 208.62 (CO), 213.89 (d, J_{PC} = 5.2 Hz, CO) ppm. ³¹P{¹H} NMR (202.46 MHz, CDCl₃/CS₂ (v/v = 1/1), 298 K): 93.31 (s) ppm. FAB⁺-MS: m/z 1298.9 {**1**}⁺, 1241.9 {**1** - 2CO}⁺, 1159.0 {**1** - 5CO}⁺. Anal. Calcd for C_{87.4}H_{24.8}Fe₂O₅PS_{2.4}: C, 76.38; H, 1.82. Found: C, 76.36; H, 1.89.

Reduction of $[(\mu\text{-bdt})\text{Fe}_2(\text{CO})_5(\text{C}_{60}(\text{H})\text{PPh}_2)]$ by cobaltcene. A red-brown suspension of **1** (60 mg, 0.046 mmol) in 12 mL of THF was generated at $-70\text{ }^\circ\text{C}$ and a solution of Cp_2Co (9 mg, 0.048 mmol) in 2 mL THF was added dropwise. The resulting dark red-brown solution was stirred for 5 minutes and monitored by in situ FTIR spectroscopy. The red-shifted ν_{CO} IR bands by $\sim 5\text{ cm}^{-1}$ confirmed formation of $[\text{Cp}_2\text{Co}][\mathbf{1}]$. The single-electron reduced product remained stable at low temperature for at least one hour. Addition of cold hexane to the concentrated solution of $[\text{Cp}_2\text{Co}][\mathbf{1}]$ afforded the red-brown solid. A significant amount of the product was lost during precipitation. The yield of the reduced product was 30 % (20 mg). IR (THF, cm^{-1}): ν_{CO} 2047 (vs), 1990 (vs), 1978 (s), 1938 (w).

Reaction of $[(\mu\text{-bdt})\text{Fe}_2(\text{CO})_5(\text{C}_{60}(\text{H})\text{PPh}_2)]$ with Na and dibenzo-18-crown-6 ether.

To a THF solution (4 mL) containing Na metal (100 mg, 4.35 mmol) at $-90\text{ }^\circ\text{C}$ was added via cannula the red-brown THF suspension (4 mL) of **1** (22 mg, 0.017 mmol) that was pre-cooled to $-90\text{ }^\circ\text{C}$. Dibenzo-18-crown-6 ether (15 mg, 0.057 mmol) was dissolved in 1 mL of THF solution first and then added dropwise to the reaction flask containing **1** and Na. The reaction temperature was kept below $-60\text{ }^\circ\text{C}$. A green solution was slowly generated with disappearance of **1**. It was monitored by in situ FTIR spectroscopy. Formation of $[\text{dibenzo-18-crown-6-Na}][(\mu\text{-bdt})\text{Fe}_2(\text{CO})_5(\text{C}_{60}\text{PPh}_2)]$, $[\text{dibenzo-18-crown-6-Na}][\mathbf{3}]$, was confirmed by the ν_{CO} bands: 2044 (vs), 1986 (vs), 1972 (s), 1934 (w) cm^{-1} .

Reaction of $[(\mu\text{-bdt})\text{Fe}_2(\text{CO})_5(\text{C}_{60}(\text{H})\text{PPh}_2)]$ with KO^tBu. To a THF solution (6 mL) of **1** (20 mg, 0.0154 mmol) and 18-crown-6 ether (4.1 mg, 0.0155 mmol) at $-50\text{ }^\circ\text{C}$ was added KO^tBu (1 M in THF, 14 μL , 0.014 mmol). The suspension was immediately

dissolved in the THF solution and the color changed to green. The solution was stirred for 10 minutes and checked by in situ FTIR spectroscopy. Formation of [18-crown-6-ether-K][$(\mu\text{-bdt})\text{Fe}_2(\text{CO})_5(\text{C}_{60}\text{PPh}_2)$], [18-crown-6-ether-K][**3**], was confirmed by the ν_{CO} bands shifted to lower energy. Addition of cold hexane to the concentrated solution of [18-crown-6-ether-K][**3**] afforded the green solid. A significant amount of the product was lost during precipitation. The yield of the reduced product was 41 % (10 mg). IR (THF, cm^{-1}): ν_{CO} 2048 (vs), 1991 (vs), 1977 (s), 1934 (w).

Synthesis of $(\mu\text{-bdt})\text{Fe}_2(\text{CO})_5(\text{PPh}_3)$, **2.** To a CH_2Cl_2 solution (8 mL) of $(\mu\text{-bdt})\text{Fe}_2(\text{CO})_6$ (200 mg, 0.48 mmol) was slowly added an CH_3CN solution (5 mL) of Me_3NO (36 mg, 0.48 mmol). An instant color change was observed from red to dark red-brown. The solution was stirred an hour and then was concentrated to about one third of the volume. It was transferred to a Schlenk flask containing PPh_3 (131 mg, 0.5 mmol) via cannula. Additional 10 mL of CH_2Cl_2 was added and the solution was stirred for half an hour. The solution was evaporated to dryness and the resultant red solid was washed by hexane a few times prior to being dried. The yield was 267 mg (85 %). IR (CH_2Cl_2 , cm^{-1}): ν_{CO} 2051 (vs), 1992 (vs), 1983 (s, sh), 1937 (w). ^1H NMR (500 MHz, CDCl_3 , 298 K): 6.18 (m, 2H, $\text{S}_2\text{C}_6\text{H}_4$), 6.50 (s, 2H, $\text{S}_2\text{C}_6\text{H}_4$), 7.35 (m, 9H, $\text{P}(\text{C}_6\text{H}_5)_3$), 7.49 (m, 6H, $\text{P}(\text{C}_6\text{H}_5)_3$) ppm. $^{13}\text{C}\{^1\text{H}\}$ NMR (125.7 MHz, CDCl_3 , 297 K): 125.40 (s, 2C, $\text{S}_2\text{C}_6\text{H}_4$), 127.63 (s, 2C, $\text{S}_2\text{C}_6\text{H}_4$), 128.52 (d, 6C, $J_{\text{PC}} = 9.6$ Hz, $\text{P}(\text{C}_6\text{H}_5)_3$), 130.03 (s, 3C, $\text{P}(\text{C}_6\text{H}_5)_3$), 133.36 (d, 6C, $J_{\text{PC}} = 11.2$ Hz, $\text{P}(\text{C}_6\text{H}_5)_3$), 135.98 (d, 3C, $J_{\text{PC}} = 40.1$ Hz, *ipso*- $\text{P}(\text{C}_6\text{H}_5)_3$), 148.26 (s, 2C, *ipso*- $\text{S}_2\text{C}_6\text{H}_4$), 209.38 (s, 3C, CO), 213.83 (d, 2C, $J_{\text{PC}} = 7.4$ Hz, CO) ppm. $^{31}\text{P}\{^1\text{H}\}$ NMR (202.46 MHz, CDCl_3 , 296 K): 62.68 (s) ppm. FAB+-MS: m/z 514.1 {**2** –

$5\text{CO} + \text{H}^+\}^+$, 598.0 $\{\mathbf{2} - 2\text{CO} + \text{H}^+\}^+$, 655.0 $\{\mathbf{2} + \text{H}^+\}^+$. Anal. Calcd for $\text{C}_{29.9}\text{H}_{21}\text{Cl}_{0.6}\text{Fe}_2\text{O}_5\text{PS}_2$: C, 52.17; H, 3.08. Found: C, 52.13; H, 2.98.

II. Table

Table S1. X-ray Crystallographic Data

	1·CS₂	2
Empirical formula	C ₈₄ H ₁₅ Fe ₂ O ₅ PS ₄	C ₂₉ H ₁₉ Fe ₂ O ₅ PS ₂
Formula weight	1374.87	654.23
<i>T</i> , K	150(2)	150(2)
Crystal system	Monoclinic	Triclinic
Space group	<i>P</i> 2 ₁ / <i>c</i>	P-1
<i>a</i> , Å	11.1324(2)	10.6019(6)
<i>b</i> , Å	18.2639(3)	12.1058(7)
<i>c</i> , Å	25.9839 (4)	13.0037(7)
α , °	90	64.5114(10)
β , °	100.0104(6)	66.7002(11)
γ , °	90	68.1529(11)
<i>V</i> , Å ³	5202.64(15)	1341.99(13)
<i>Z</i>	4	2
ρ_{calcd} , Mg m ⁻³	1.755	1.619
μ , mm ⁻¹	0.819	1.336
<i>F</i> (000)	2760	664
Reflections collected	30850	17816
Independent reflections	11894	6150
<i>R</i> _{int}	0.0388	0.0280
Goodness-of-fit on <i>F</i> ²	1.055	1.028
R1 [<i>I</i> > 2σ(<i>I</i>)] (all data) ^a	0.0468 (0.0735)	0.0296 (0.0338)
wR2 [<i>I</i> > 2σ(<i>I</i>)] (all data) ^b	0.1291 (0.1407)	0.0695 (0.0718)

^a $R1 = (\sum||F_o| - |F_c||) / (\sum|F_o|)$. ^b $wR2 = [\sum w(F_o^2 - F_c^2)^2 / \sum w(F_o^2)^2]^{1/2}$.

Table S2. List of the electrochemical data.

Complex	Solution	E (V) ^a	Ref
[(μ -bdt)Fe ₂ (CO) ₆]	CH ₃ CN	-1.32 ^c	d
	CH ₃ CN	-1.27 ^c	e
	CH ₂ Cl ₂	-1.44 ^c	f
	CH ₂ Cl ₂ / <i>o</i> -DCB (v/v 1:1)	-1.50 ^c	This work
[(μ -bdt)Fe ₂ (CO) ₅ (PTA)]	CH ₃ CN	-2.0	g
[(μ -bdt)Fe ₂ (CO) ₅ (C ₆₀ (H)PPh ₂)], 1	CH ₂ Cl ₂ / <i>o</i> -DCB (v/v 1:1)	-1.1, ^b -1.48, ^b -1.78, ^c -2.14 ^c	This work
[(μ -bdt)Fe ₂ (CO) ₅ (PPh ₃)], 2	CH ₂ Cl ₂ / <i>o</i> -DCB (v/v 1:1)	-1.87	This work

^a $E = E_{pc}$ for irreversible waves and $E_{1/2}$ when reversible. All potentials are against Fc/Fc⁺. ^b reversible events at room temperature. ^c reversible events at low temperature. ^d Felton, G. A. N.; Vannucci, A. K.; Chen, J.; Lockett, L. T.; Okumura, N.; Petro, B. J.; Zakai, U. I.; Evans, D. H.; Glass, R. S.; Lichtenberger, D. L. *J. Am. Chem. Soc.* **2007**, *129*, 12521-12530. ^e Capon, J.-F.; Gloaguen, F.; Schollhammer, P.; Talarmin, J. J. *Electroanal. Chem.* **2006**, *595*, 47-52. ^f Capon, J.-F.; Gloaguen, F.; Schollhammer, P.; Talarmin, J. J. *Electroanal. Chem.* **2004**, *566*, 241-247. ^g Vannucci, A. K.; Wang, S.; Nichol, G. S.; Lichtenberger, D. L.; Evans, D. H.; Glass, R. S. *Dalton Trans.* **2010**, *39*, 3050-3056.

III. Figures

Figure S1. Molecular structure of $[(\mu\text{-bdt})\text{Fe}_2(\text{CO})_5(\text{PPh}_3)]$, **2**. Hydrogen atoms are omitted for clarity. Selected bond length (\AA) and angles (deg): Fe–Fe, 2.4917(4); Fe–S, 2.2812(5); Fe–C_{CO,ap}, 1.806(2); Fe–C_{CO,ba}, 1.780(2); Fe–P, 2.2530(5); S–Fe–S, 80.140(18); S–Fe–Fe, 56.897(14); Fe–S–Fe, 66.206(15). There is a pi-pi interaction between the dithiolate bridge and the coordinated triphenylphosphine. The shortest plane-to-plane distance is 3.162 \AA .

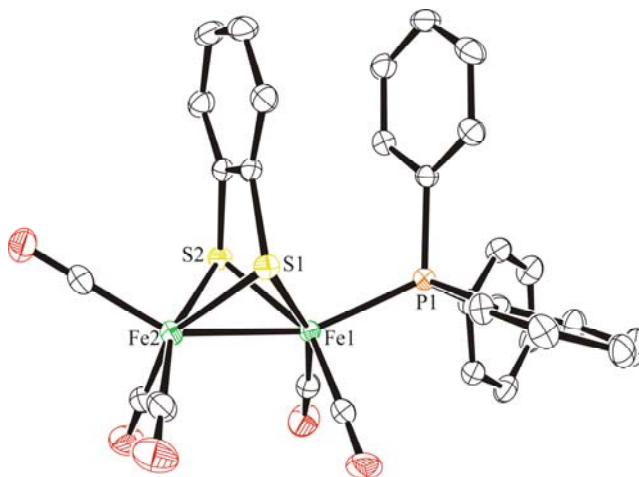


Figure S2. Cyclic voltammograms of **1** in the anodic region. (the $\text{CH}_2\text{Cl}_2/o\text{-DCB}$ solution, 1 mM, 256 K, $\nu = 100 \text{ mV/s}$, 0.1 M $n\text{-Bu}_4\text{NPF}_6$).

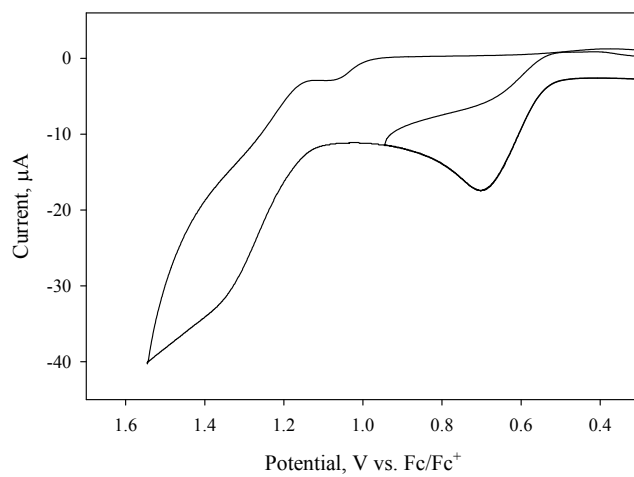


Figure S3. Cyclic voltammogram of $[(\mu\text{-bdt})\text{Fe}_2(\text{CO})_6]$ in the $\text{CH}_2\text{Cl}_2/o\text{-DCB}$ solution. (1 mM, 298 K, $\nu = 100 \text{ mV/s}$, 0.1 M $n\text{-Bu}_4\text{NPF}_6$).

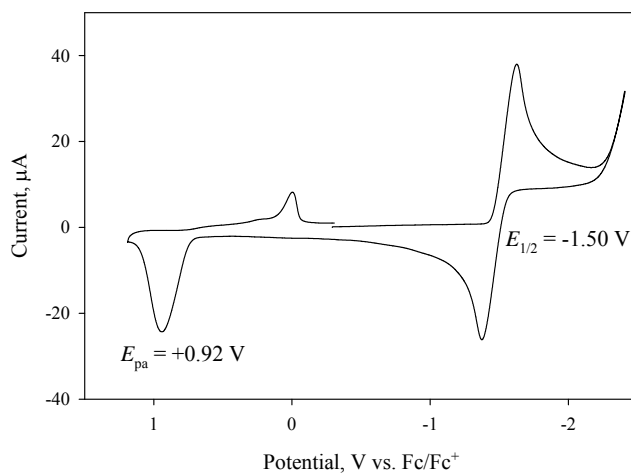


Figure S4. IR spectra of **1** (black) and $[1]^-$ (blue) in THF solution at $-50\text{ }^\circ\text{C}$.

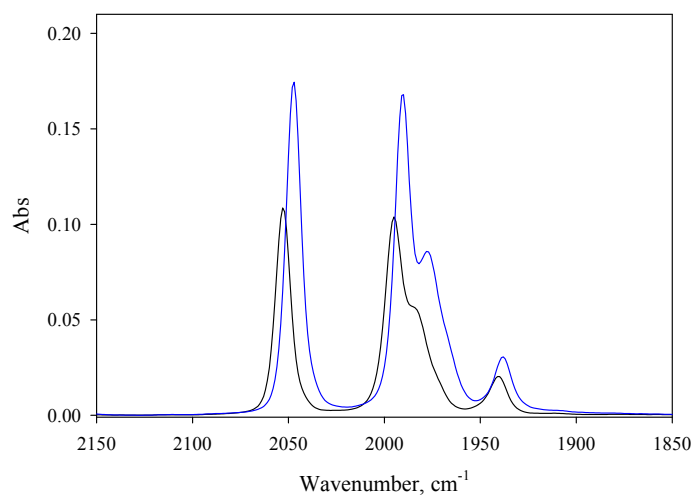
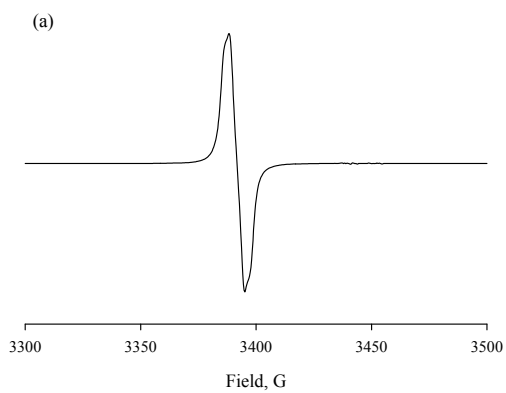


Figure S5. 77 K EPR spectra of (a) $[1]^-$ and (b) $[3]^-$ in THF. The in-situ vis-near IR spectra of (c) $[1]^-$ and (d) $[3]^-$ in THF at $-70\text{ }^\circ\text{C}$.



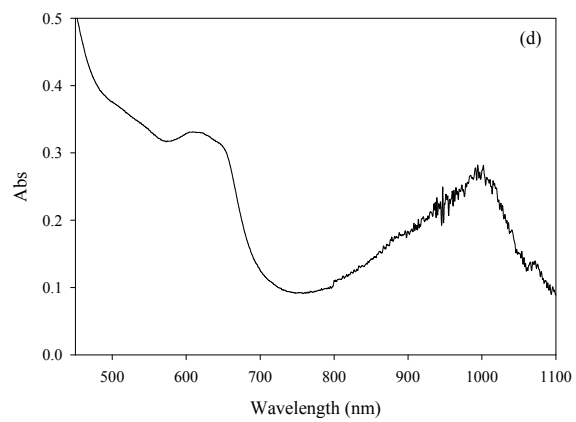
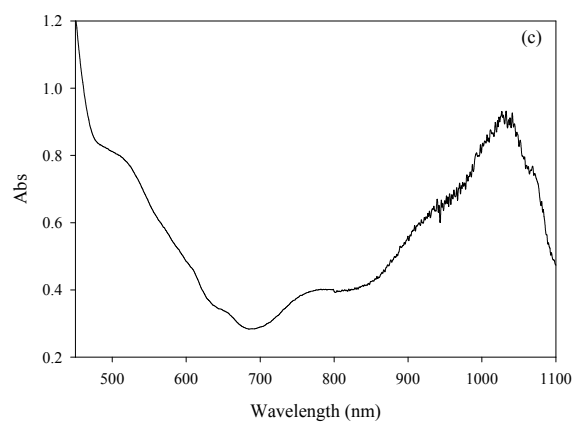
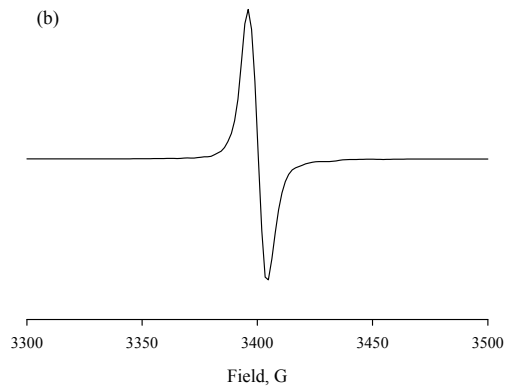


Figure S6. The vis-NIR spectral change of $[1]^{+}$ upon addition of 2 equiv of acids in the THF solution at $-50\text{ }^{\circ}\text{C}$: (a) HCl and (b) HOAc. The transition at 710 nm marked as an asterisk (*) is a feature of **1**. The lines in black and blue represent the spectra in the absence and presence of acids, respectively.

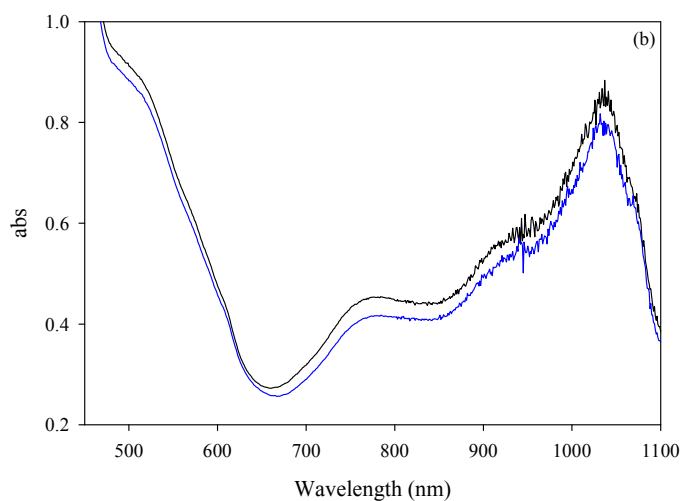
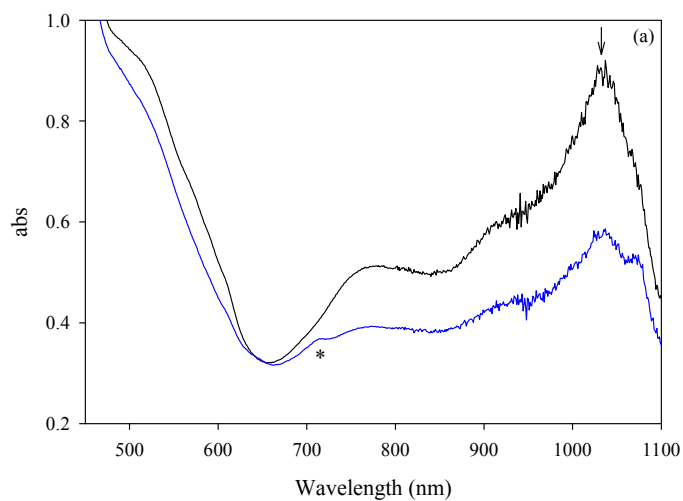
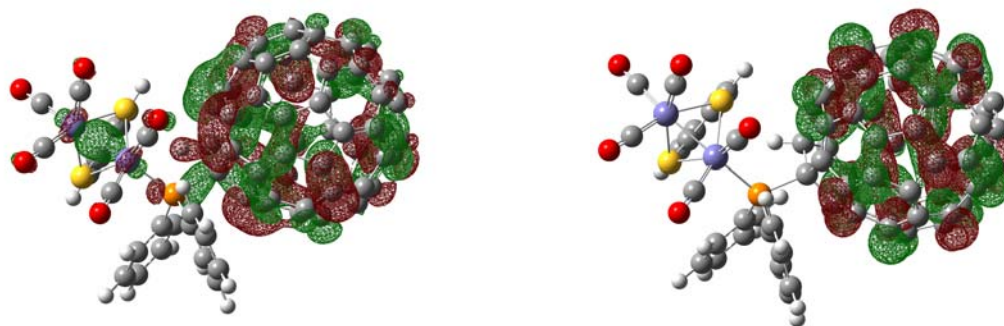


Figure S7. (a) The results of **1** from the DFT calculations: (a1) the HOMO and LUMO (a2) the computed orbital energies of the frontier orbitals (a3) the computed results of selected structural parameters. (b) The results of $[1]^{+}$ from the DFT calculations: (b1) the computed orbital energies of the frontier orbitals (b2) the computed results of selected structural parameters. (c) The results of $[1]^{2-}$ from the DFT calculations: (c1) the HOMO and LUMO of the singlet state (c2) the computed orbital energies of the frontier orbitals of the singlet state (c3) the computed orbital energies of the frontier orbitals of the triplet state (d) The predicted IR spectra for **1**, $[1]^{+}$, and the singlet and triplet states of $[1]^{2-}$. IR intensities (in km/mol) are shown in the parentheses.

For the complex **1**: (a1) HOMO (left) and LUMO (right)



(a2)

	in hartree (in eV)
LUMO+2	-0.105 (-2.86)
LUMO+1	-0.115 (-3.13)
LUMO	-0.118 (-3.21)
HOMO	-0.211 (-5.74)
HOMO-1	-0.215 (-5.85)

HOMO-2	-0.217 (-5.90)
--------	----------------

(a3)

	bond length (Å)
Fe-Fe	2.448
Fe(distal)-S	2.328, 2.331
Fe(proximal)-S	2.352, 2.357
Fe-P	2.295

For the complex $[1]^{+-}$: (b1)

Alpha orbitals	in hartree (in eV)
LUMO+1	-0.003 (-0.08)
LUMO	-0.012 (-0.33)
HOMO	-0.043 (-1.17)
HOMO-1	-0.107 (-2.91)
HOMO-2	-0.109 (-2.97)
HOMO-3	-0.111 (-3.02)

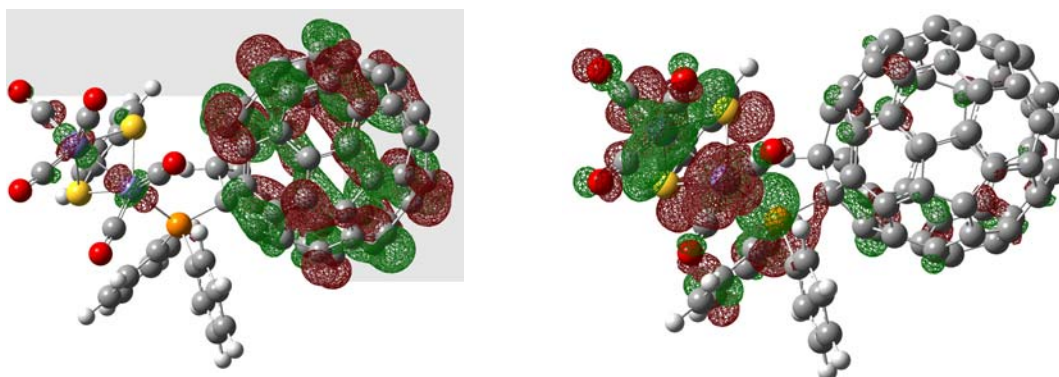
Beta orbitals	in hartree (in eV)
LUMO+2	-0.003 (-0.08)
LUMO+1	-0.009 (-0.24)
LUMO	-0.011 (-0.30)
HOMO	-0.104 (-2.83)

HOMO-1	-0.104 (-2.83)
HOMO-2	-0.107 (-2.91)

(b2)

	bond length (Å)
Fe-Fe	2.456
Fe(distal)-S	2.328, 2.333
Fe(proximal)-S	2.352, 2.354
Fe-P	2.314

For the complex $[1]^{2-}$: for the singlet state (c1) HOMO (left) and LUMO (right)



(c2)

	in hartree (in eV)
LUMO+2	+0.080 (+2.18)
LUMO+1	+0.070 (+1.90)
LUMO	+0.056 (+1.52)
HOMO	-0.003 (-0.08)
HOMO-1	-0.007 (-0.19)

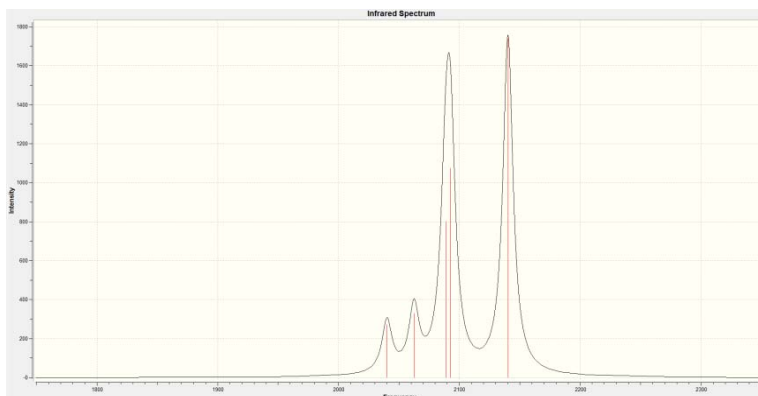
HOMO-2	-0.011 (-0.30)
--------	----------------

For the triplet state: (c3)

Alpha orbitals	in hartree (in eV)
LUMO	0.056 (+1.52)
HOMO	+0.025 (+0.68)
HOMO-1	+0.022 (+0.60)
HOMO-2	-0.036 (-0.98)
HOMO-3	-0.041 (-1.12)
HOMO-4	-0.042 (-1.14)

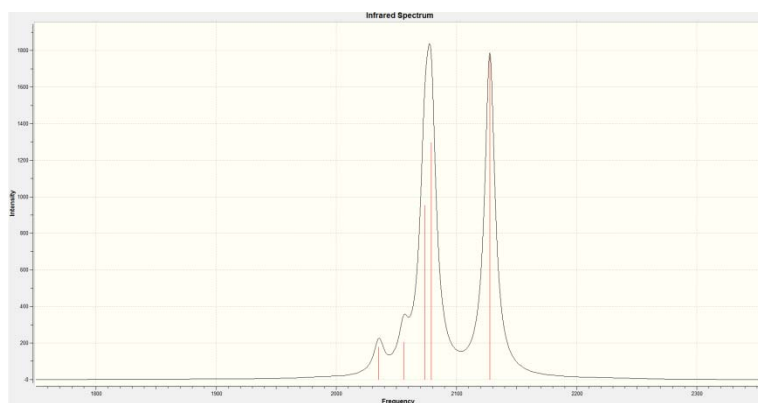
Beta orbitals	in hartree (in eV)
LUMO+2	+0.066 (+1.80)
LUMO+1	+0.057 (+1.55)
LUMO	+0.054 (+1.47)
HOMO	-0.001 (-0.03)
HOMO-1	-0.034 (-0.93)
HOMO-2	-0.035 (-0.95)

(d) The computed v_{CO} for **1**:



ν_{CO} : 2040 (270); 2062 (328); 2088 (800); 2092 (1074); 2140 (1737)

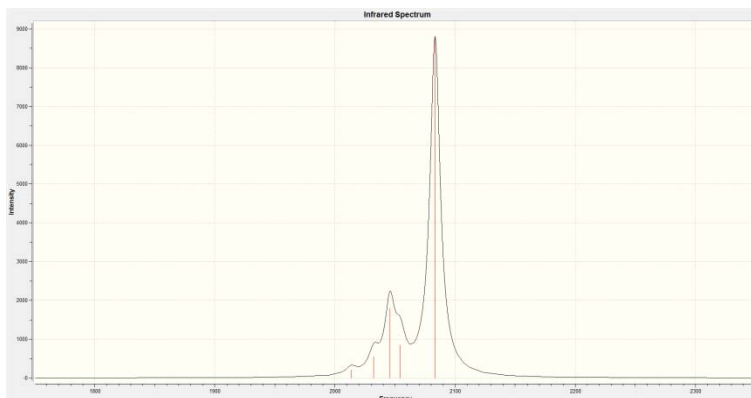
The computed ν_{CO} for $[\mathbf{1}]^{\bullet-}$:



ν_{CO} : 2035 (178); 2056 (204); 2073 (952); 2078 (1295); 2127 (1765)

For the computed ν_{CO} bands, $[\mathbf{1}]^{\bullet-}$ is higher in energy than $\mathbf{1}$ by av. 11 cm^{-1} .

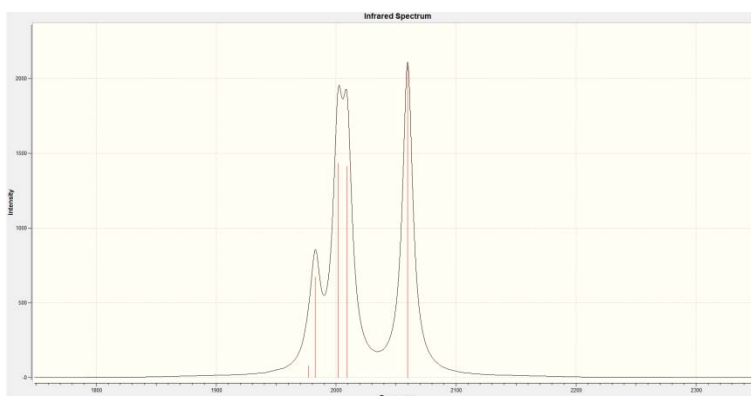
The computed ν_{CO} for the singlet state of $[\mathbf{1}]^{2-}$:



ν_{CO} : 2013 (207); 2032 (546); 2045 (1799); 2054 (847); 2083 (8751)

For the computed ν_{CO} bands, the singlet state of $[\mathbf{1}]^{2-}$ is higher in energy than $\mathbf{1}$ by av. 39 cm^{-1} .

The computed ν_{CO} for the triplet state of $[\mathbf{1}]^{2-}$:



ν_{CO} : 1976 (79); 1982 (673); 2001 (1433); 2009 (1411); 2059 (2083)

For the computed ν_{CO} bands, the triplet state of $[\mathbf{1}]^{2-}$ is higher in energy than $\mathbf{1}$ by av. 79 cm^{-1} .

Figure S8 . Cyclic voltammograms of **2** in the $\text{CH}_2\text{Cl}_2/o\text{-DCB}$ solution. (1 mM, 275 K, $\nu = 100$ mV/s, 0.1 M $n\text{-Bu}_4\text{NPF}_6$).

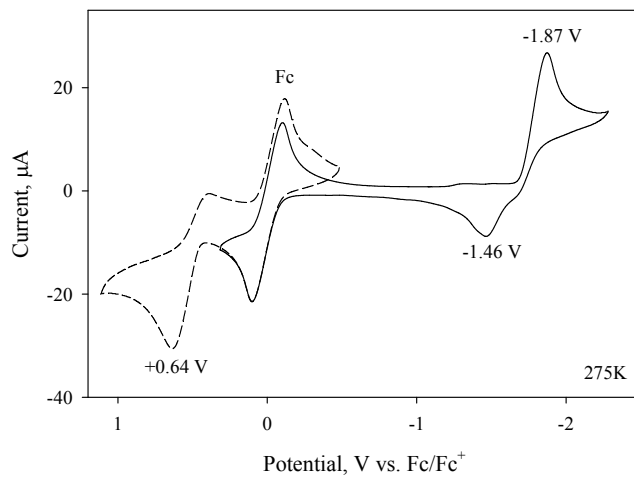
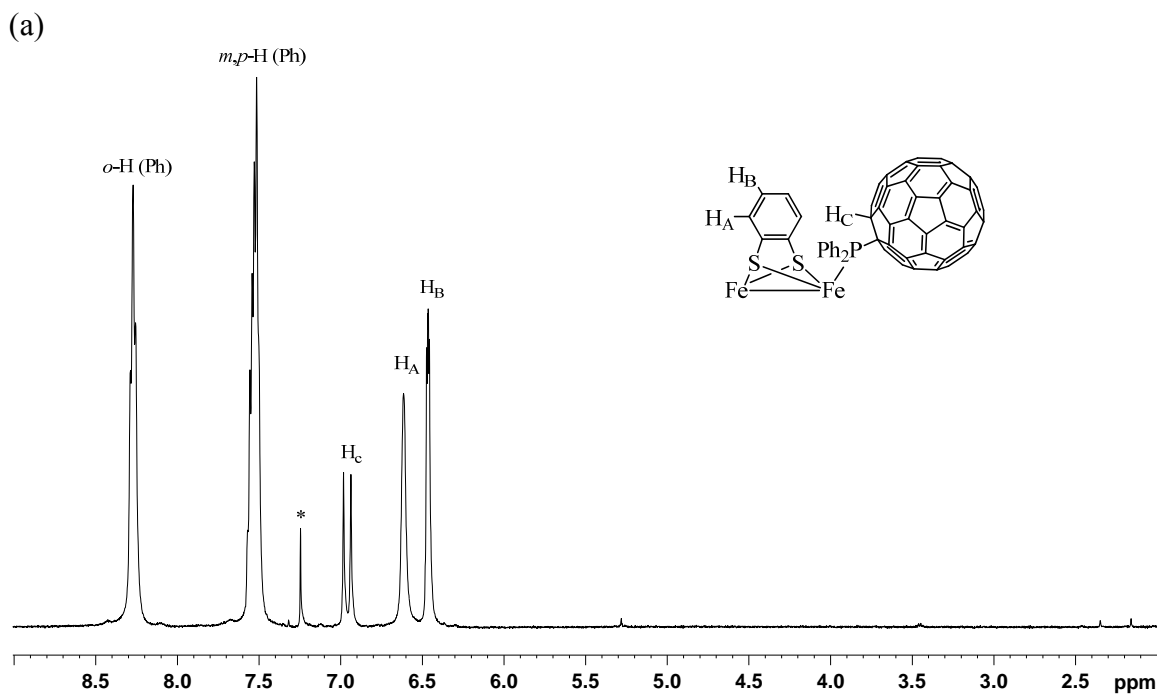
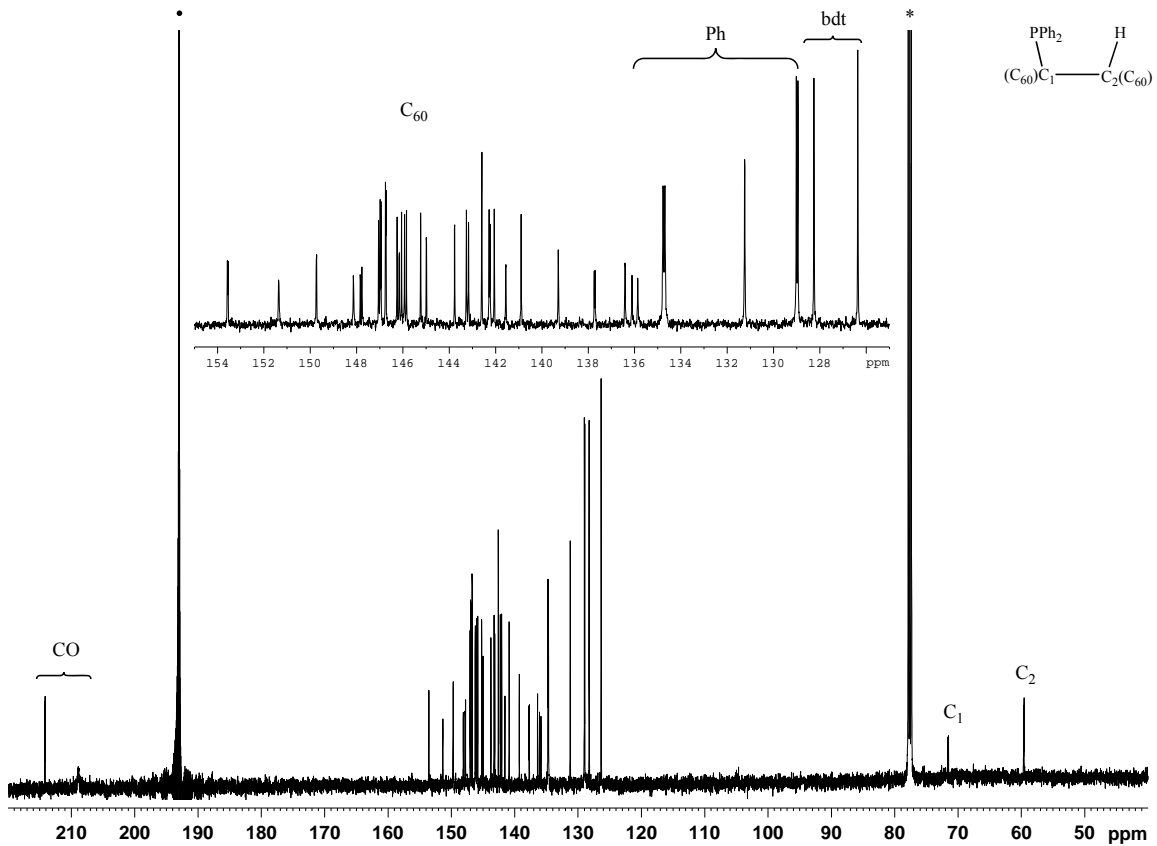


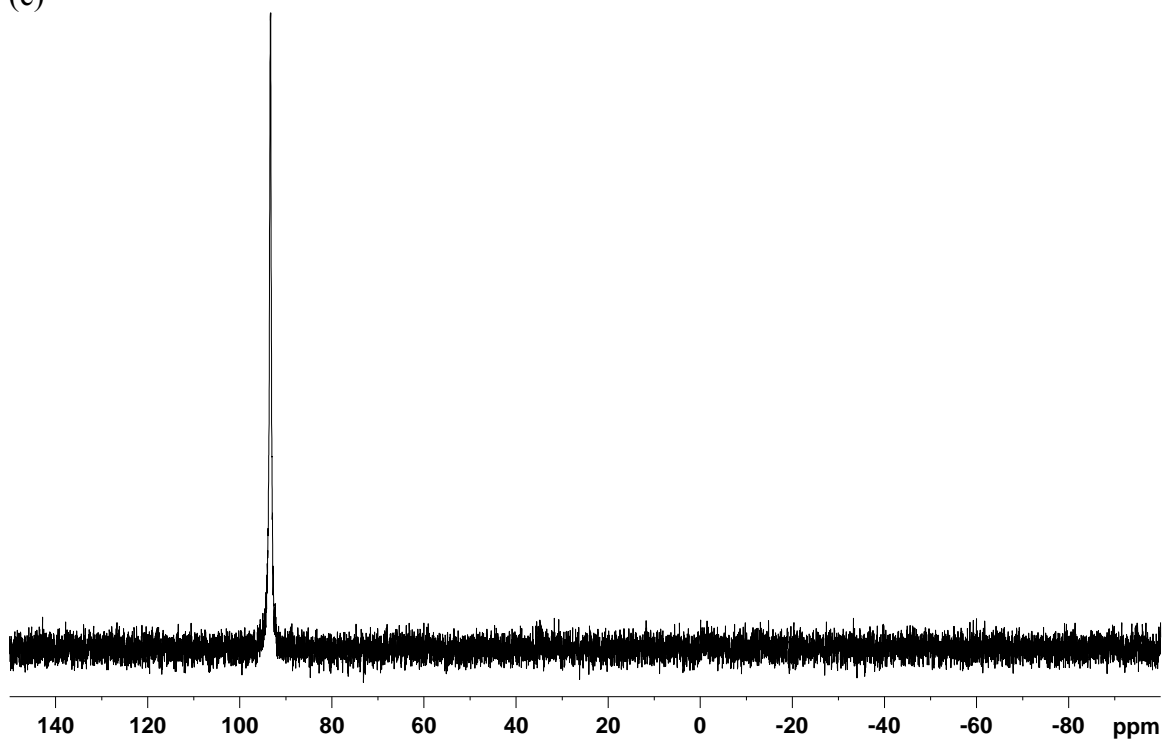
Figure S9. NMR spectra of **1** in the CS₂/CDCl₃ (v/v 1/1) solution at 298 K: (a) ¹H-NMR spectrum (b) ¹³C-NMR spectra (c) ³¹P-NMR spectrum. Solvent signals from CDCl₃ and CS₂ are marked as an asterisk (*) and a bullet (•), respectively.



(b)



(c)



References

- (1) Cabeza, J. A.; Martinez-Garcia, M. A.; Riera, V.; Ardura, D.; Garcia-Granda, S. *Organometallics* **1998**, *17*, 1471-1477.
- (2) Yamago, S.; Yanagawa, M.; Mukai, H.; Nakamura, E. *Tetrahedron* **1996**, *52*, 5091-5102.
- (3) *SHELXTL*, ver. 6.10; Bruker Analytical X-Ray Systems: Madison, WI, 2000.
- (4) Becke, A. D. *J. Chem. Phys.* **1993**, *98*, 5648-5652.
- (5) Lee, C.; Yang, W.; Parr, R. G. *Phys. Rev. B* **1988**, *37*, 785-789.
- (6) Frisch, M. J. T., G. W.; Schlegel, H. B.; Scuseria, G. E.; Robb, M. A.; Cheeseman, J. R.; Montgomery Jr., J. A.; Vreven, T.; Kudin, K. N.; Burant, J. C.; Millam, J. M.; Lyengar, S. S.; Tomasi, J.; Barone, V.; Mennucci, B.; Cossi, M.; Scalmani, G.; Rega, N.; Petersson, G. A.; Nakatsuji, H.; Hada, M.; Ehara, M.; Toyota, K.; Fukuda, R.; Hasegawa, J.; Ishida, M.; Nakajima, T.; Honda, Y.; Kitao, O.; Nakai, H.; Klene, M.; Li, X.; Knox, J. E.; Hratchian, H. P.; Cross, J. B.; Adamo, C.; Jaramillo, J.; Gomperts, R.; Stratmann, R. E.; Yazyev, O.; Austin, A. J.; Cammi, R.; Pomelli, C.; Ochterski, J.; Ayala, P. Y.; Morokuma, K.; Voth, G. A.; Salvador, P.; Dannenberg, J. J.; Zakrzewski, V. G.; Dapprich, S.; Daniels, A. D.; Strain, M. C.; Farkas, O.; Malick, D. K.; Rabuck, A. D.; Raghavachari, K.; Foresman, J. B.; Ortiz, J. V.; Cui, Q.; Baboul, A. G.; Clifford, S.; Cioslowski, J.; Stefanov, B. B.; Liu, G.; Liashenko, A.; Piskorz, P.; Komaromi, I.; Martin, R. L.; Fox, D. J.; Keith, T.; Al-Laham, M. A.; Peng, C. Y.; Nanayakkara, A.; Challacombe, M.; Gill, P. M. W.; Johnson, B.; Chen, W.; Wong, M. W.; Gonzalez, C.; Pople, J. A. *Gaussian03*; Gaussian Inc.: Pittsburgh, PA, 2003.
- (7) Bard, A. J.; Faulkner, L. R. *Electrochemical Methods: Fundamentals and Applications*; John Wiley & Sons: New York, 1980.